American Mineralogist, Volume 75, pages 620–630, 1990

Fe-rich pyroxenes from a microdiorite dike, Whangarei, New Zealand

RAYMOND N. BROTHERS†
Department of Geology, University of Auckland, Private Bag, Auckland, New Zealand
KAZUMI YOKOYAMA
Department of Geology, National Science Museum, Hyakunin-cho, 3-23-1, Shinjuku-ku, Tokyo, 160 Japan

ABSTRACT

Pyroxenes in a microdiorite dike near Whangarei, New Zealand, formed during cooling from magmatic temperatures >900 °C to nearly subsolidus temperatures at about 700 °C, with development of Fe-rich compositions between hypersthene and orthoferrosilite, between augite and hedenbergite, and around Fe-rich pigeonite. Orthoferrosilite ($Fs_{92}En_4Wo_4$) forms partial rims on crystals that contain zoning from Mg-rich to Fe-rich orthopyroxene. Pigeonite, with Fe/(Mg + Fe) > 0.70, crystallized on augite and ferroan augite or as separate interstitial grains and is rarely mantled by ferroan amphibole. Textures and compositions indicate that the Fe-enriched minerals were late products, or the latest products, during crystallization of the microdiorite. Fe-rich pigeonite and orthoferrosilite were metastable phases that grew mainly as epitaxial overgrowths on early-stage pyroxenes during rapid cooling near 850–700 °C and 700 °C, respectively.

INTRODUCTION

Near Whangarei, New Zealand, basement Permian-Jurassic prehnite-pumpellyite metagraywackes have been intruded by a Lower Miocene microdiorite dike that outcrops on the seacoast near Matapouri anad can be traced inland for 20 km in a remarkably straight line through 13 outcrops (Fig. 1). The dike maintains a width of about 15 m and has developed a 1- to 2-m contact aureole of fine-grained hornblende-biotite hornfels in the graywacke country rocks. Details of the local geology and field localities are given by Brothers (1989).

The microdiorite is part of a mid-Tertiary calc-alkaline igneous province that covers large areas in the northern North Island (Brothers, 1986) and forms a thick subaerial basaltic andesite-dacite sequence at Whangarei Heads (Fig. 1). Samples from the 13 main dike outcrops show very little variation in whole-rock chemistry and a restricted range of SiO_2, 59.81–61.20 wt%; an average of the analyses and CIPW norms is in Table 1. In comparison with andesites and a diorite with similar SiO_2 contents from the nearby Whangarei Heads calc-alkaline suite, the microdiorite has higher contents of Fe_2O_3 + FeO (Fig. 2), which reflect the presence of the Fe-enriched pyroxenes described in this paper.

Pyroxenes are common among silicate minerals, and their phase relations have been studied experimentally in some detail (e.g., Huebner and Turnock, 1980; Lindsley and Anderson, 1983). Within the pyroxene quadrilateral there is a "forbidden zone" (Lindsley and Munoz, 1969) where pyroxenes are not stable at low pressure and where phase relations of natural systems are enigmatic, especially when crystallized under conditions of rapid cooling. Few igneous pyroxenes formed at low pressure have compositions lying within the forbidden zone and close to the hedenbergite-orthoferrosilite join (Bowen, 1935; Bown, 1965; Klein et al., 1971).

Mg-rich pigeonite is not uncommon in volcanic and intrusive rocks, but experiments show that orthoferrosilite and Fe-rich pigeonite with Fe/(Mg + Fe) > 0.70 are metastable at low pressure (Lindsley and Anderson, 1983). Orthoferrosilite is stable only at elevated pressures and has been reported from high-grade metamorphic terrains (Jaffe et al., 1978; Katsushima, 1985). Similarly, Fe-rich pigeonite (X_{Fe} > 0.7) is thought to have formed at high pressure within the Nain anorthosite massif and to have decomposed to Fe-rich hypersthene and Fe-rich augite during regional uplift (Smith, 1974). Under low-pressure conditions the assemblage olivine–quartz–Fe-rich augite is the stable equivalent of Fe-rich pigeonite-orthoferrosilite.

In contrast to previous evidence, this paper presents data for extreme iron enrichment in pyroxenes with Fe-rich pigeonite and orthoferrosilite compositions that coexisted in a microdiorite dike. As a narrow linear body, located close to an area of coeval subaerial eruptions, the dike apparently was emplaced and cooled in a high-level low-pressure environment.

DIKE PETROGRAPHY

Apart from narrow 20-cm chilled margins on the dike, all the microdiorite samples in thin section have similar mineral assemblages in fine- to medium-grained holocrystalline associations of plagioclase with subordinate amounts of pyroxenes, biotite, ilmenite, and quartz. Pot-

† Deceased, May 1988.

0003–004X/90/0506–0620$02.00

Fig. 1. Regional geology and outcrop localities for the Matapouri microdiorite dike.

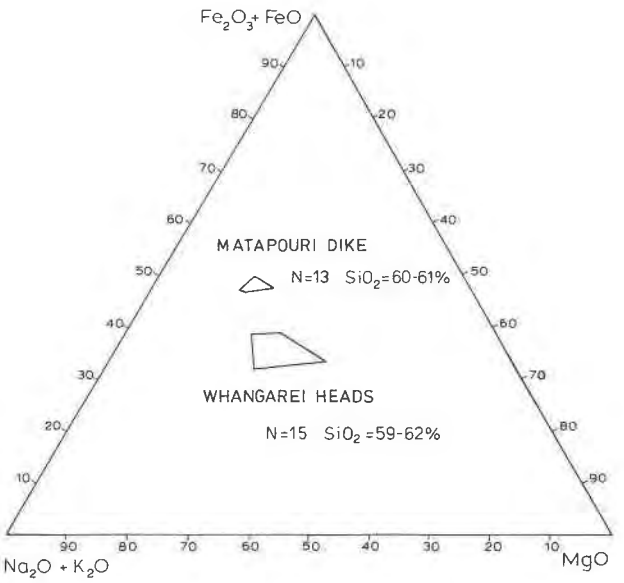

Fig. 2. AFM whole-rock compositions for the Matapouri microdiorite dike and for comparable rocks in the coeval Whangarei Heads calc-alkaline volcanic field (Fig. 1) from Middleton (1983).

ash feldspar and acicular apatite are invariably present in small quantities, and amphibole in minor amounts occurs in most thin sections. All of the observed brown micaceous minerals are biotite that is microscopically intergrown with, and replaced by, chlorite. Ca-rich chabazite is an interstitial alteration phase and commonly fills cavities or cracks in plagioclase, quartz, and pyroxene. Oxides are dominantly ilmenite, which includes plagioclase (An_{85-79}) and glass and is itself sometimes enclosed by pyroxenes. Titanomagnetite postdates the ilmenite, which it surrounds in aggregates, and is marginally altered to maghemite. Sulphides are rare occurrences of pyrrhotite, pyrite, marcasite, and chalcopyrite; there are no replacements of oxides by sulphides. Carbonates are mainly acicular siderite in radiating aggregates and calcite that is interstitial with chabazite.

The dike margins are strongly porphyritic with pyroxene and plagioclase prisms surrounded by mordenite that has completely replaced an originally silica-rich glass matrix. In contrast to the main body of the dike, these chill zones lack amphibole, biotite, potash feldspar, and quartz. They have only a restricted range of compositional zonation in plagioclase and Fe-rich pyroxenes and represent an important identifiable stage in the sequence of intrusion and crystallization.

Mineral chemistry

Chemical analyses of the minerals were carried out on a Link Systems energy-dispersive spectrometer, using natural and synthetic materials as standards with corrections by the ZAF method of Statham (1979). Precision and detection limits of the analyses with the EDS and ZAF are similar to those obtained by Dunham and Wilkinson (1978, 1980). All the analyses were made under the back-scattered electron image, and no exsolution phases were observed in any minerals. Representative analyses are in Table 2. Compositions of the pyroxenes and of pyroxene pairs at their contacts are plotted in Ca-Mg-Fe diagrams as Figure 3 and Figure 4, respectively.

Orthopyroxene. Although they sometimes occur in radiating aggregates (Fig. 5A), orthopyroxenes generally are prisms elongated parallel to **c**, up to 1-mm long and 0.3-mm wide, with included ilmenite or, rarely, plagioclase and glassy phases (now replaced by chabazite). Orthopyroxene cores often show oscillatory zoning with hypersthene compositions (X_{Fe} = 0.35–0.45), but in most samples strong iron enrichment is usually present toward the margins and particularly in the direction of the **c** axis,

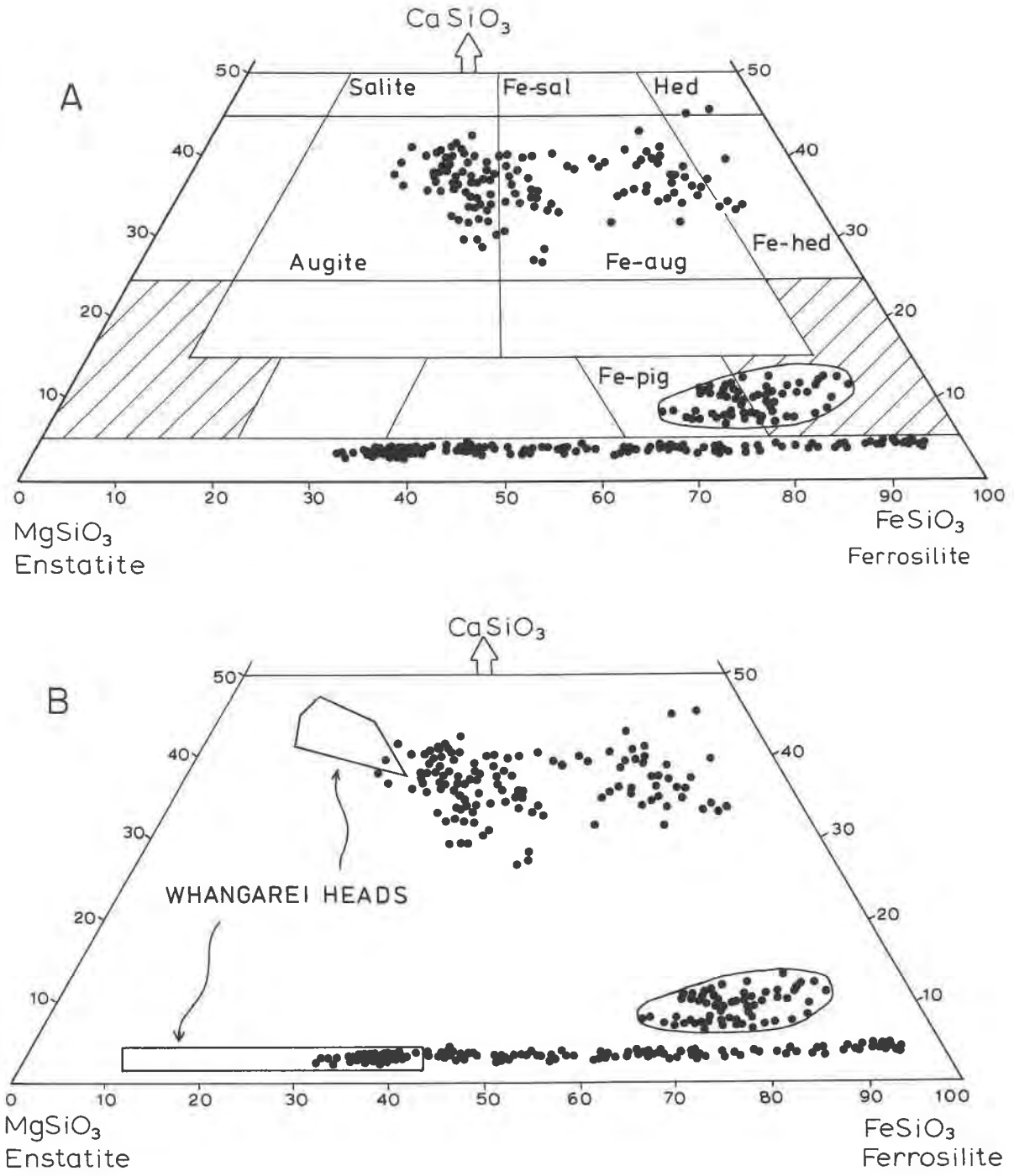

Fig. 3. Pyroxene compositions in the Matapouri dike. (A) In relation to the compositional fields of Poldervaart and Hess (1951). (B) Comparison with pyroxenes in the adjacent coeval Whangarei Heads calc-alkaline field (from Middleton, 1983). (C) Pyroxene compositions in the chilled margin of the dike.

where rims commonly have X_{Fe} = 0.70–0.80. The total core-to-rim variation for orthopyroxenes from all localities is $En_{65}Fs_{32}Di_3$ to $En_4Fs_{92}Di_4$ (Fig. 3), the most Fe-rich orthoferrosilite being found in an amphibole-free sample. These compositions are distributed linearly in the Ca-Mg-Fe diagram (Fig. 3) with a wollastonite content of 3.0–3.5 mol% on the Mg side and 4.0–5.0 mol% at the Fe end. Minor oxides in the pyroxenes are MnO

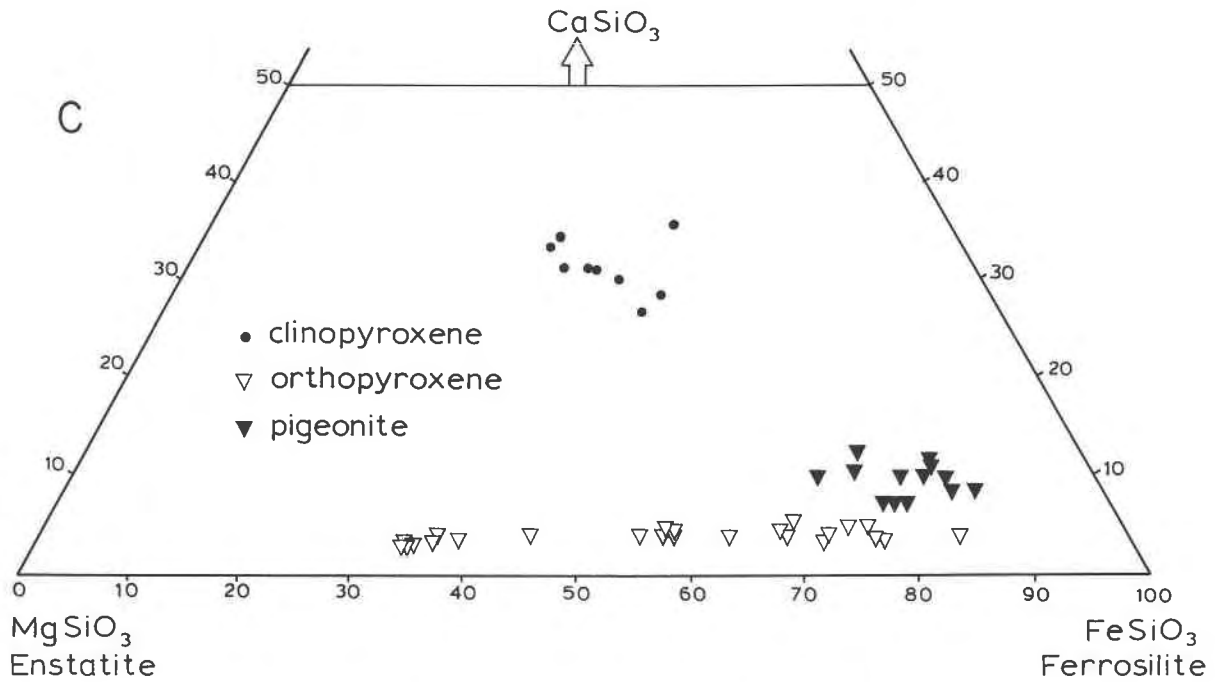

and Al_2O_3; with Fs increase, the MnO content rises slightly from 0.3 to 1.0 wt%, but Al_2O_3 decreases from 1.4 to 0.5 wt%.

Discrete orthopyroxene crystals commonly have overgrowths of Ca-rich clinopyroxenes (Fig. 5B, 5C), but only in the directions of the **a** and **b** axes where the host crystal shows no notable zoning, so that both phases have low X_{Fe} at their contact. In contrast, discrete orthopyroxene without Ca-rich overgrowths is zoned to ferro-hypersthene or eulite margins in the **a** and **b** directions. This type of compositional change is usually continuous from core to rim, but discontinuous zoning can be seen along crystal cracks (Fig. 5D) where orthopyroxene with $X_{Fe} > 0.50$ has grown on an early phase with $X_{Fe} = 0.30$–0.40. This relationship indicates crystallization of Fe-rich pyroxenes after the development of partings in an older generation of pyroxenes.

Ca-rich pyroxene. The main occurrence of Ca-rich pyroxene is as overgrowths on orthopyroxene; it only rarely occurs as discrete grains. In both modes the grain size is less than 0.2 mm, and the crystals have oscillatory zoning. Ca-rich pyroxenes in contact with orthopyroxene are augites, with Fe/(Mg + Fe) ratios of 0.40–0.55, which carry partial mantles of Fe-rich augite, hedenbergite, or Fe-rich pigeonite on their **a** and **b** directions (Fig. 5B, 5C). Compositional variation from augite to Fe-rich augite is discontinuous, and Fe-rich augite occasionally forms a lining on partings in early-crystallized augite (Fig. 5E). Wollastonite contents in the augites are variable between 27 and 42 mol%, despite apparent equilibration with the orthopyroxene.

Pigeonite. Fe-enriched pigeonite was seen in half of the samples, occurring mainly around augite and rarely as overgrowths on orthopyroxene or as separate interstitial tabular grains. The composition range is Fe/(Mg + Fe) = 0.70–0.92, with Wo content near 10 mol% at contacts with augite and near 7 mol% in contact with orthopyroxene and in a discrete crystal. Fe-rich pigeonite overgrown on augite is mantled sometimes by ferroan hornblende.

Feldspar. Plagioclase is usually less than 1 mm in size and is phenocrystic within the microdiorite. The cores commonly have oscillatory zoning with compositions of An_{87-78}, which pass outwards to An_{60}, where there is usually an abrupt change to K-enriched oligoclase at $An_{15}Ab_{70}Or_{15}$, outside of which there is a final partial rim

Table 1. Averages of 13 whole-rock analyses and their CIPW norms

SiO_2 =	60.51(0.40)	Q =	15.21(1.48)
TiO_2 =	0.95(0.04)	C =	0.28(0.23)
Al_2O_3 =	17.74(0.13)	Or =	12.33(0.54)
Fe_2O_3 =	1.18(0.03)	Ab =	25.66(3.10)
FeO =	5.92(0.16)	An =	27.89(2.33)
MnO =	0.16(0.02)	Di =	0.11(0.27)
MgO =	2.47(0.20)	Hy =	14.70(0.53)
CaO =	5.82(0.51)	Mt =	1.72(0.05)
Na_2O =	3.03(0.37)	Il =	1.80(0.08)
K_2O =	2.09(0.09)	Ap =	0.31(0.02)
P_2O_5 =	0.14(0.01)		100.01
	100.01		

Note: Averages are in wt%, with standard deviations in parentheses. All analyses have been normalized to 100% volatile-free, with Fe_2O_3/FeO set to 0.20.

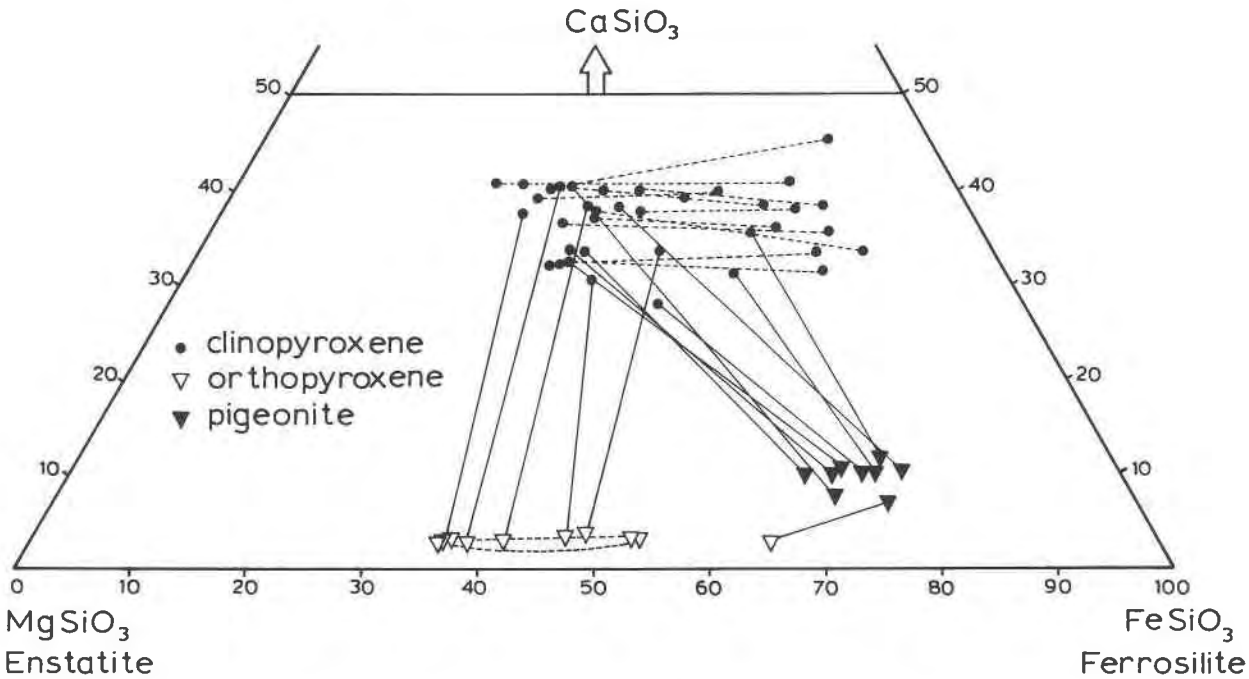

Fig. 4. Ca-Mg-Fe plot of pyroxene compositions. Solid tie lines indicate compositions at contacts between core grains and overgrowths. Broken lines indicate abrupt changes of composition within pyroxenes, for example, adjacent to cracks (see Fig. 5D, 5E).

TABLE 2. Representative microprobe analyses of pyroxenes and amphiboles

Mineral	Orthopyroxene				Pigeonite		
SiO_2	52.34	49.50	47.05	45.84	48.67	47.72	46.92
TiO_2	0.38	0.33	0.29	0.23	0.17	0.15	0.10
Al_2O_3	1.37	1.33	1.25	0.46	0.65	0.97	0.75
FeO*	21.14	31.94	40.94	48.64	38.25	41.97	43.46
MnO	0.30	0.64	0.98	1.02	0.91	1.00	1.12
MgO	22.93	14.07	6.81	1.39	7.14	4.42	2.47
CaO	1.50	1.76	1.72	1.70	4.53	4.97	5.07
Total	99.96	99.57	99.04	99.28	100.32	101.20	99.89
Fe	33.1	53.9	74.0	91.4	67.4	74.7	80.0
Mg	63.9	42.3	22.0	4.6	22.4	14.0	8.1
Ca	3.0	3.8	4.0	4.0	10.2	11.3	11.9

Mineral	Calcic pyroxene				Amphibole		
SiO_2	52.62	50.21	49.18	48.34	44.58	45.37	49.71
TiO_2	0.37	0.51	0.25	0.24	0.58	0.31	0.27
Al_2O_3	0.85	2.34	1.36	0.98	7.23	4.13	1.28
FeO*	13.82	21.31	27.49	30.51	29.76	31.69	30.18
MnO	0.48	0.38	0.39	0.73	0.27	1.03	3.02
MgO	14.64	9.37	5.59	4.98	4.50	3.66	2.75
CaO	17.68	16.48	15.42	14.09	9.66	8.89	10.80
Na_2O	0.56	0.35	0.53	0.35	1.41	1.60	0.58
K_2O					0.40	0.56	0.23
Total	101.02	100.95	100.21	100.22	98.39	97.24	98.82
Fe	22.1	36.1	48.1	53.2	59.3	63.9	61.7
Mg	41.7	28.2	17.4	15.4	16.0	13.1	10.0
Ca	36.2	35.7	34.5	31.4	24.7	23.0	28.3

* Total Fe as FeO.

of sodic K-feldspar at $Or_{75}Ab_{25}$ (Fig. 6). A few crystals show compositions that span the entire range.

Another set of plagioclase and potash feldspars have different compositions and textures and belong to a post-igneous stage of recrystallization (Fig. 6). Albite-oligoclase, with very low Or content, mantles plagioclase or replaces An_{87-78} cores in association with chabazite. Similarly, a Na-poor K-feldspar ($>Or_{95}$) with euhedral external facets replaces the sodic K-feldspar ($Or_{75}Ab_{25}$), as shown in Figure 5F, or forms discrete interstitial crystals.

Amphibole. Amphibole has grown on clinopyroxene, or formed rectangular interstitial prisms, with compositions between ferroan hornblende and ferro-actinolite (Fig. 7A, 7B) and with Fe/(Mg + Fe) ratios like those of Fe-rich pigeonite, Fe-rich augite, and hedenbergite. Amphibole compositions show a gradual change in $^{[4]}$Al and Na + K along the length of the dike (Fig. 7B). During mid-Miocene regional tectonism, postdating the calc-alkalic volcanism, the graywacke basement was uplifted and tilted toward the southwest (Brothers, 1989). Since the dike is sub-vertical and northeast trending, the northeastern outcrops (localities 1–5) represent originally deeper parts of the intrusive body. Amphiboles that crystallized at the deeper levels, presumably at higher pressure than localities 6–10, contain more $^{[4]}$Al and Na + K.

Other minerals. Biotite could not be analyzed with confidence because of the extensive alteration to chlorite,

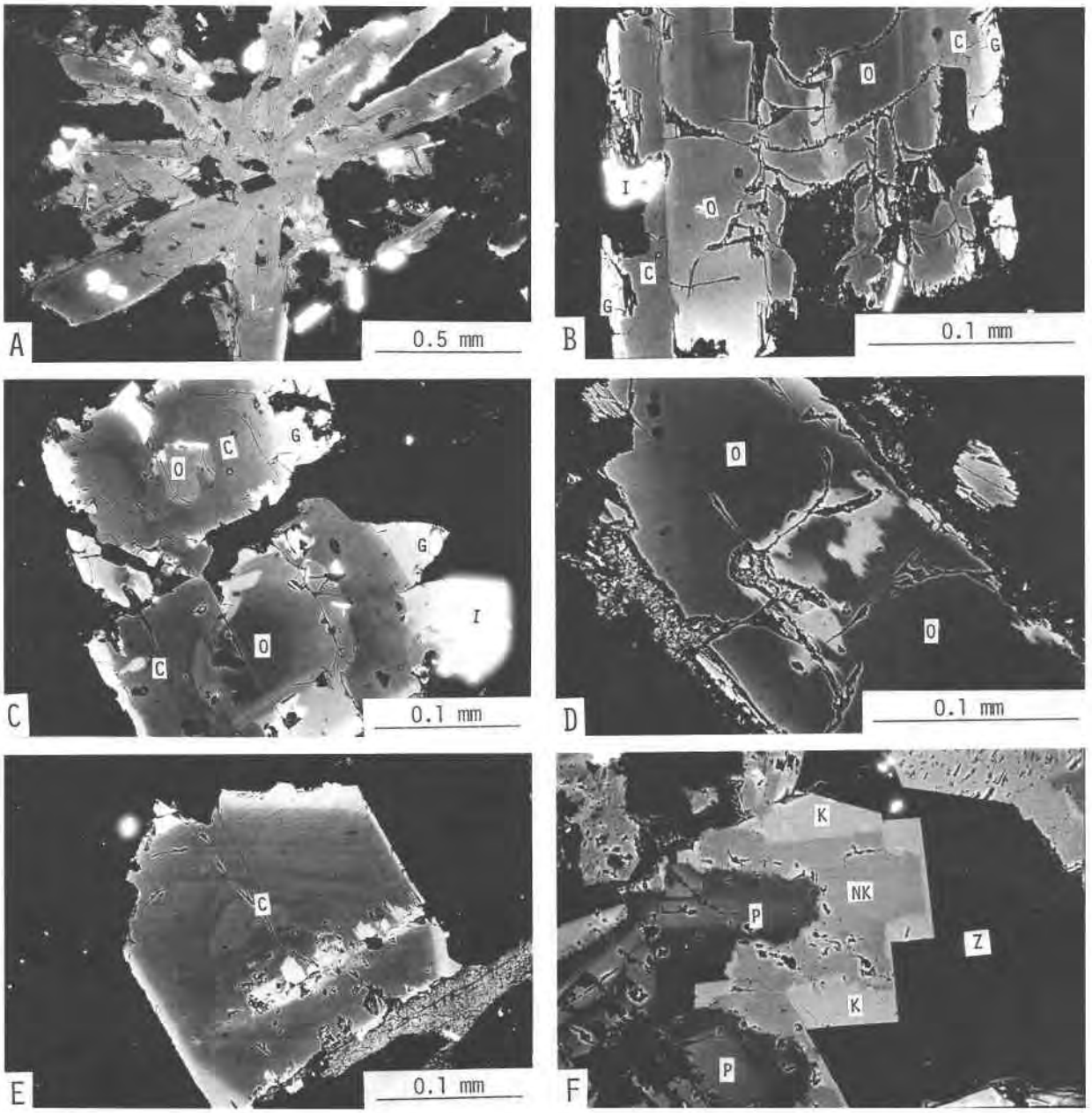

Fig. 5. Back-scattered electron images of mineral textures and compositions in the Matapouri dike. Strong iron enrichment (light colors) is present commonly at the rims of pyroxenes. (**A**) Radiating aggregate of orthopyroxene (Fs_{32-82}) in sample 38669. (**B**) Orthopyroxene, subparallel to the **c** axis, with overgrowths of calcic pyroxene and ferro-pigeonite, sample 38669. (**C**) Orthopyroxene, perpendicular to the **c** axis, with overgrowths of calcic pyroxene and Fe-rich pigeonite, sample 38668. (**D**) Fe-rich orthopyroxene formed along a crack in early-stage hypersthene, sample 38677. (**E**) Fe-rich augite formed along a crack in early augite, sample 38148. (**F**) Post-igneous Na-poor K-feldspar with euhedral facets replacing sodic K-feldspar. Abbreviations: O = orthopyroxene, C = calcic pyroxene, G = pigeonite, I = ilmenite, NK = sodic K-feldspar, K = Na-poor K-feldspar, Z = zeolite, P = plagioclase.

which is evident in microdomains where the potash loss has been balanced by crystallization of K-feldspar ($>Or_{95}$). Less altered biotite intergrown with chlorite has Fe/(Mg + Fe) ratios near 0.80.

Chilled sample. At locality 9, a chilled margin on the dike (sample 36050) contains a mineral assemblage that lacks amphibole and has restricted ranges of composition in feldspar and pyroxenes. This assemblage records a stage in the crystallization of the dike (Fig. 8) when the magmatic body had intruded the graywacke basement up to

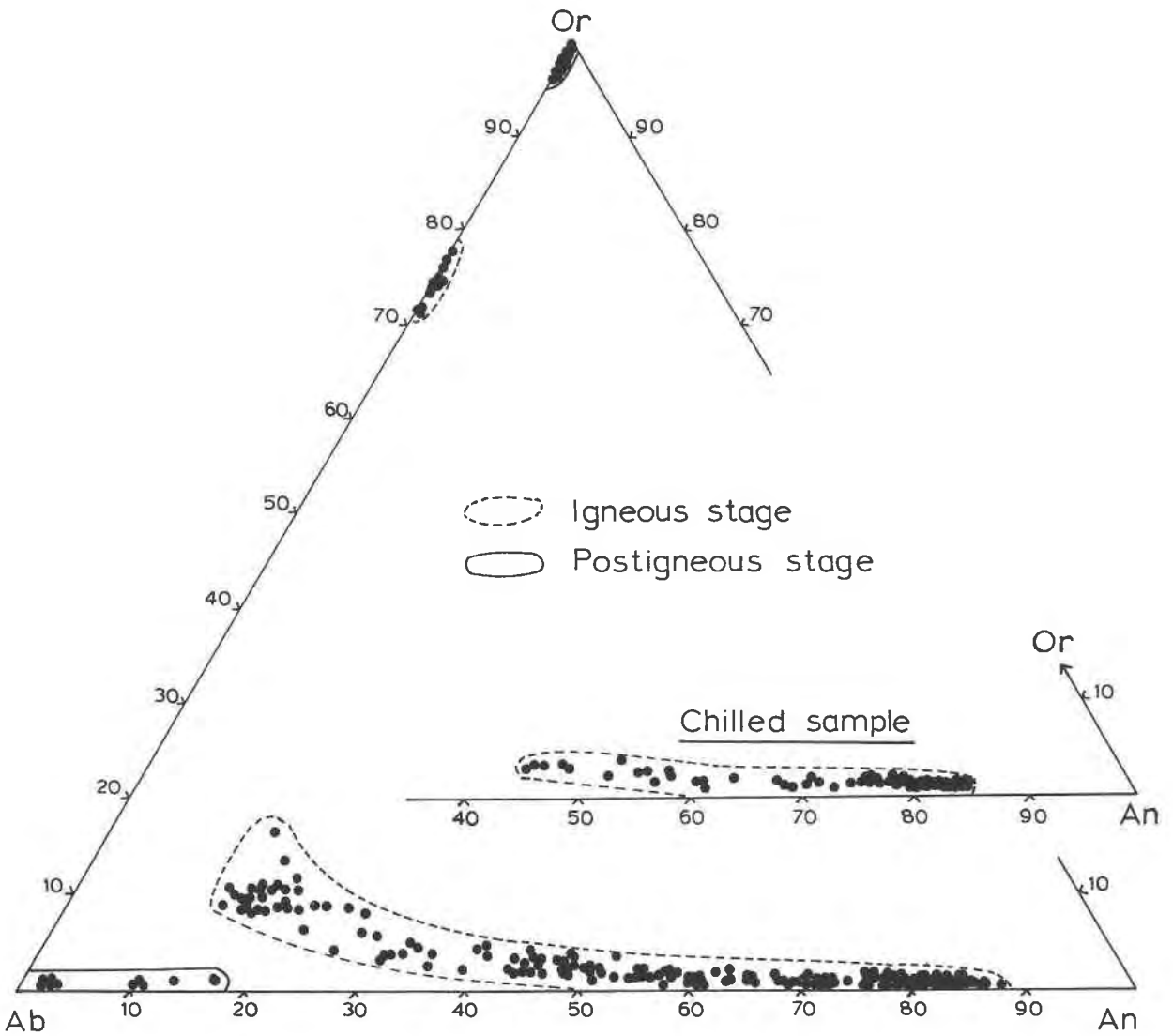

Fig. 6. Compositional ranges of feldspar formed at the igneous and post-igneous stages. In the chilled margin of the dike only plagioclase feldspar is present.

the level of locality 9. Pyroxenes in the chilled margin (Fig. 3C) were iron-enriched but do not display the wider compositional range or the extreme iron enrichment found in pyroxenes from central parts of the dike (Fig. 3A, 3B). Similarly, plagioclase in the chilled margin has a restricted anorthite content, An_{85-45} (Fig. 6), and albite and potash feldspars are absent.

Discussion

Crystallization sequence

The textures and chemical compositions of the mineral assemblage indicate that plagioclase crystallized first and was followed by hypersthene and ilmenite and then augite (Fig. 8). The plagioclase and pyroxenes have patterns of oscillatory zoning that are also found in comparable phenocrysts in volcanic rocks (e.g., Clark et al., 1986) but differ in their textures. The microdiorite pyroxenes are elongate or coarsely spherulitic, and overgrowths of augite on hypersthene are crystallographically controlled, suggesting that the early-stage minerals crystallized more rapidly than most large phenocrysts in volcanic rocks (Lofgren, 1974).

Fe-rich pyroxenes occur within early-stage Mg-rich pyroxenes along cracks that must have developed before the crystallization of Fe-rich augite and Fe-rich pigeonite. Such discontinuous changes in composition within the pyroxenes, as well as pronounced zoning toward plagioclase and pyroxene margins, indicate an abrupt change in physical conditions that probably caused the onset of magma quenching. Thus, it is likely that the intracrystal cracks were formed at a time of uprise, or dike formation,

of the microdiorite magma and were followed by crystallization of Fe-rich orthopyroxene, Fe-rich augite, and Fe-rich pigeonite, mainly as epitaxial additions to early-stage Mg-rich pyroxenes (Fig. 8). In rapidly cooled rocks, Ca-rich pyroxenes commonly have sector zoning, with discontinuous compositional trends across sectoral boundaries. Similar features are seen in some augites of the microdiorite.

Orthoferrosilite and hedenbergite were later crystallates, nucleating only as overgrowths on orthopyroxene and augite, respectively. X_{Fe} of the mafic minerals and compositions of mineral inclusions suggest that biotite, oligoclase ($An_{15}Ab_{70}Or_{15}$), sodic K-feldspar ($Or_{75}Ab_{25}$), amphibole, and quartz crystallized at a late, or even the latest, stage of igneous solidification.

During post-igneous alteration, magmatic minerals and their interstices were replaced by chabazite or mordenite, K-feldspar ($>Or_{95}$), albite-oligoclase (Ab_{100} to $Ab_{80}An_{20}$), siderite, and chlorite.

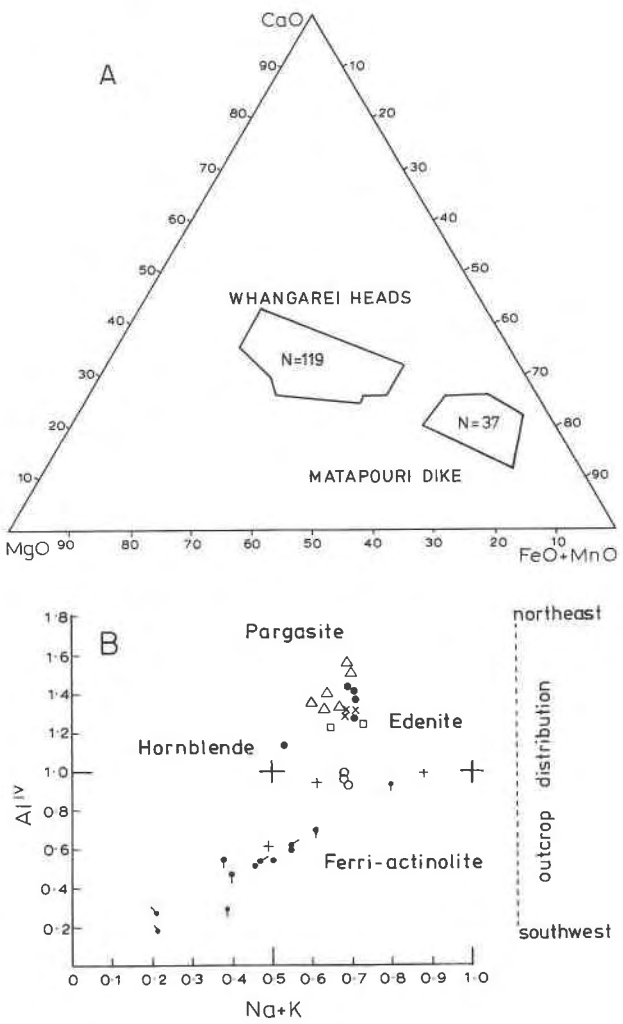

Fig. 7. Amphibole compositions in the Matapouri dike. (**A**) Compared with amphiboles from the Whangarei Heads calc-alkaline field (Middleton, 1983). (**B**) Compositions along the length of the dike, showing depletion in $^{[4]}Al$ and Na + K trending northeast; each of the ten outcrops is represented by a separate symbol.

Temperature conditions

The compositions of coexisting pyroxenes can be used as a geothermometer for crystallization. Since the microdiorite solidified in a near-surface setting, pyroxene phase relations at low pressure (Lindsley and Anderson, 1983) should be applicable. It may be optimistic to use such equilibrium diagrams to determine temperatures within a petrographically defined mineral sequence in an intrusive body as small as the Matapouri microdiorite. Nevertheless, when phase parameters from Lindsley and Anderson (1983) are used to assess the Matapouri data, the deduced temperatures are reasonable and are supported by plagioclase compositions and by mineral assemblages at the late stage of igneous crystallization.

The CaO content in early-stage orthopyroxene indicates that the attendant crystallization temperature was above 900 °C (Fig. 9). Although CaO contents in augite are variable and metastable crystallization during rapid cooling may be important, the augite compositions and the absence of Mg-rich pigeonite are compatible with the temperature estimate of 900 °C. The earliest microdiorite pigeonite has Fe/(Fe + Mg) = 0.70, giving a temperature near 850 °C, according to Lindsley and Anderson (1983), which is reasonably consistent with the method using CaO content in orthopyroxene having a similar Fe ratio. When one uses CaO values in Fe-rich orthopyroxene, the latest igneous temperature is near 700 °C, and at that stage the main phases to crystallize were quartz, sodic K-feldspar, potassic oligoclase, and biotite, as in a granite assemblage. The compositions of coexisting oligoclase and sodic K-feldspar in the microdiorite appear compatible with the figure of 650 °C indicated by the experimental data of Petersen and Lofgren (1986). Such estimated crystallization temperatures are not unreasonable for the microdiorite dike, despite the evidence for rapid cooling and the persistence of metastable pyroxenes with compositions lying within the forbidden zone.

For the orthopyroxenes, the regular increase of CaO content relative to the ferrosilite component (Fig. 3) is consistent with a steady decrease in temperature and continued equilibrium relations within the enstatite-ferrosilite system. In contrast, Ca-rich clinopyroxenes coexisting with the orthopyroxenes contain variable amounts of wollastonite component and are similar to Ca-rich pyroxenes in other rapidly cooled volcanics or intrusives where compositions commonly lie within an immiscibility gap between ortho- and clinopyroxenes (Hollister et al., 1971; Walker et al., 1976; Ewart, 1976). Although crystallization of pyroxenes in the microdiorite was rapid, it seems that orthopyroxenes behaved as equilibrium phases within the cooling melt as did the plagioclase feldspars.

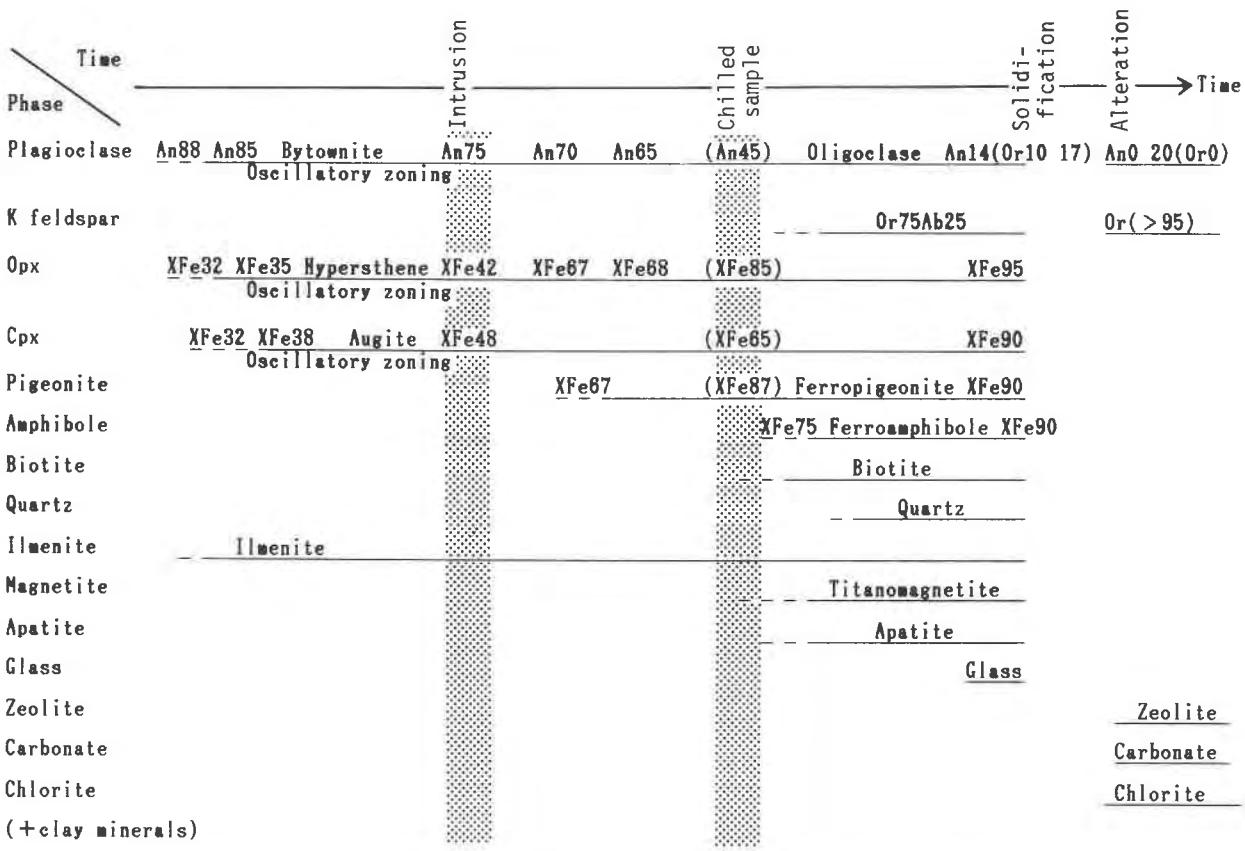

Fig. 8. Crystallization sequence of minerals in the Matapouri dike and variation in mineral composition with time.

Conclusions

The presence of Fe-rich pigeonite and orthoferrosilite is an outstanding feature of the Whangarei microdiorite, which must have crystallized at low pressures of less than 2 kbar, based on its proximity to a related coeval volcanic sequence. Rapid injection and cooling are indicated by mineral textures and compositions and by the regional setting for the dike as a long, narrow, and straight intrusion parallel to major tensional faults that developed during mid-Tertiary uplift of the graywacke basement.

The microdiorite Fe-rich pigeonites and orthoferrosilites have compositions that are unstable under low-pressure experimental conditions over a wide temperature range. However, such metastable phases are known to have crystallized under low-pressure conditions in volcanic rocks, for example, obsidian with clinoferrosilite (Bowen, 1935; Bown, 1965), lunar basalts carrying Fe-rich pigeonite, and pyroxferroite, which is stable only at high pressure (>9.5 kbar) and temperatures in excess of 1000 °C (Lindsley, 1967). Such unusual cases are restricted to quenched or rapidly cooled rocks. In slowly cooled systems, like gabbros in large layered intrusions, Fe-rich pigeonite has decomposed into orthopyroxene and Ca-rich clinopyroxene, and olivine-quartz-augite is the stable equivalent of orthoferrosilite (Wager and Brown, 1968; Smith, 1974).

Experimental studies show that diamond, a typical high-pressure mineral, can grow epitaxially on diamond nuclei at atmospheric pressure (Derjaguin et al., 1968), and pigeonites in lunar basalt are usually in epitaxial contact with augite (Bence et al., 1971). A similar epitaxic relationship is our tentative explanation for occurrences in the microdiorite of Fe-rich pigeonite and orthoferrosilite as overgrowths on Ca-rich clinopyroxene and orthopyroxene, respectively. Compositional variations of pyroxenes crystallized under supercooling conditions have been studied extensively in lunar basalts, whereas investigations into terrestrial pyroxenes have concentrated on those formed slowly or in equilibrium states, such as large crystals in volcanic rocks, layered intrusions, mantle materials, and metamorphites. Although the kinetics of crystallization in rapidly cooled rocks are not fully understood, metastable pyroxenes may be common as late-stage phases in many small intrusive bodies at high levels in the crust.

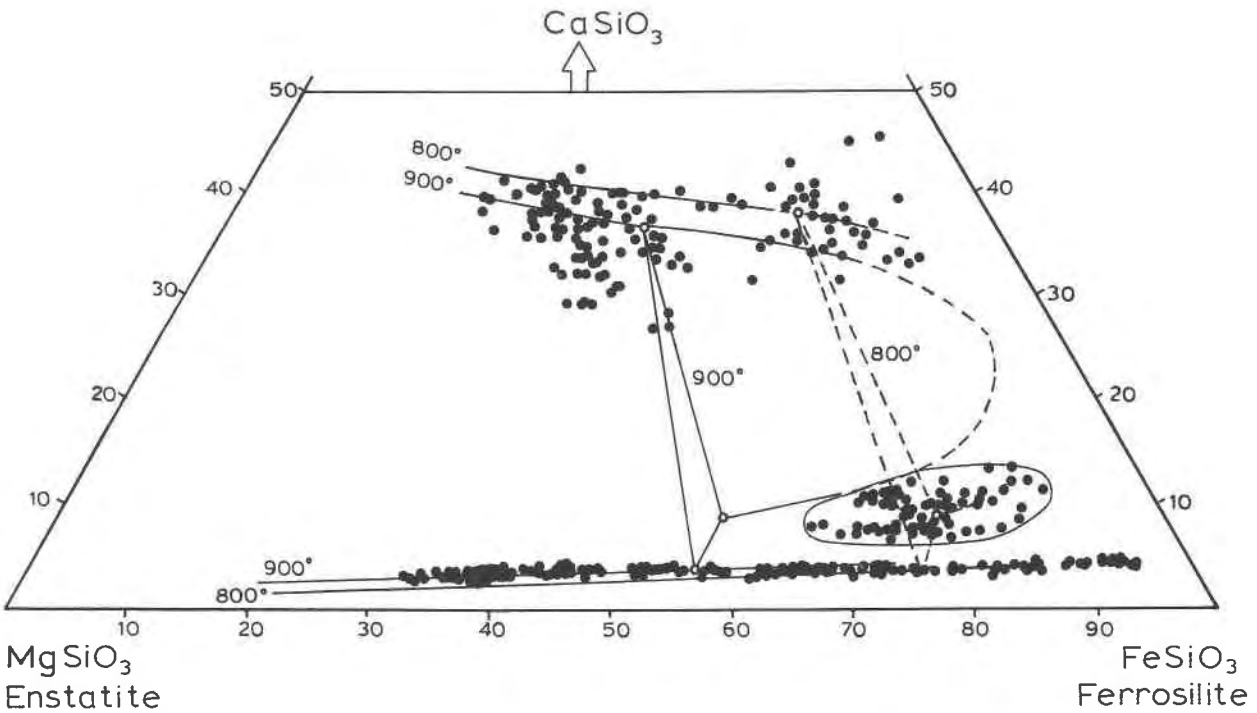

Fig. 9. Ca-Mg-Fe plot of analyzed pyroxenes from the Matapouri dike. Solid curves and tie lines show phase relations of pyroxenes at low pressure ($P < 2$ kbar) and broken lines indicate phase relations extrapolated from the high-temperature experimental data of Lindsley and Anderson (1983).

References cited

Bence, A.E., Papike, J.J., and Lindsley, D.H. (1971) Crystallization histories of clinopyroxenes in two porphyritic rocks from Oceanus Procellarum. Proceedings of the Second Lunar Science Conference, 1, 559–574.

Bowen, N.L. (1935) "Ferrosilite" as a natural mineral. American Journal of Science, 30, 481–494.

Bown, M.G. (1965) Reinvestigation of clinoferrosilite from Lake Naivasha, Kenya. Mineralogical Magazine, 34, 66–70.

Brothers, R.N. (1986) Upper Tertiary and Quaternary volcanism and subduction zone regression, North Island, New Zealand. Journal of the Royal Society of New Zealand, 16, 275–298.

——— (1989) The Matapouri-Onerahi microdiorite dike, North Island, New Zealand. New Zealand Journal of Geology and Geophysics, 32, 379–384.

Clark, A.H., Pearce, T.H., Roeder, P.L., and Wolfson, I. (1986) Oscillatory zoning and other microstructures in magmatic olivine and augite: Nomarski interference contrast observations on etched polished surfaces. American Mineralogist, 71, 734–741.

Derjaguin, B.V., Fedoseev, D.V., Lukyanovich, U.M., Spitzin, B.V., Rhyabov, V.A., and Lavrentyev, A.V. (1968) Filamentary diamond crystals. Journal of Crystal Growth, 2, 380–384.

Dunham, A.C., and Wilkinson, F.C.F. (1978) Accuracy, precision and detection limits of energy-dispersive electron-microprobe analyses of silicates. X-ray Spectrometry, 7, 50–56.

——— (1980) The suitability of energy-dispersive electron-microprobe analyses for the investigation of stainless steels. X-ray Spectrometry, 9, 8–12.

Ewart, A. (1976) A petrological study of the younger Tongan andesites and dacites, and the olivine tholeiites of Niua Fo'ou Island, S.W. Pacific. Contributions to Mineralogy and Petrology, 58, 1–21.

Hollister, L.S., Trzcienski, W.E., Jr., Hargraves, R.B., and Kulick, C.G. (1971) Petrogenetic significance of pyroxenes in two Apollo 12 samples. Proceedings of the Second Lunar Science Conference, 1, 529–557.

Huebner, J.S., and Turnock, A.C. (1980) The melting relations at 1 bar of pyroxenes composed largely of Ca-, Mg- and Fe-bearing components. American Mineralogist, 65, 225–271.

Jaffe, H.W., Robinson, P., and Tracy, R.J. (1978) Orthoferrosilite and other iron-rich pyroxenes in microperthite gneiss of the Mount Marcy area, Adirondack Mountains. American Mineralogist, 63, 1116–1136.

Katsushima, T. (1985) Granulite-facies rocks in several islands west of Langhovde, East Antarctica. Proceedings of the Fifth Symposium on Antarctic Geosciences, Memoirs of the National Institute of Polar Research, Special Issue 37, 95–110.

Klein, C., Jr., Drake, J.C., and Frondel, C. (1971) Mineralogical, petrological, and chemical features of four Apollo 12 lunar microgabbros. Proceedings of Second Lunar Science Conference, 1, 265–284.

Lindsley, D.H. (1967) The join hedenbergite-ferrosilite at high pressure and temperature. Carnegie Institution Washington Year Book, 65, 230–232.

Lindsley, D.H., and Anderson, D.J. (1983) A two-pyroxene thermometer. Journal of Geophysical Research, 88A, 887–906.

Lindsley, D.H., and Munoz, J.L. (1969) Subsolidus relations along the join hedenbergite-ferrosilite. American Journal of Science, 267A, 295–324.

Lofgren, G. (1974) An experimental study of plagioclase crystal morphology: Isothermal crystallization. American Journal of Science, 274, 243–273.

Middleton, L.M. (1983) Geology and petrology of Whangarei Heads, New Zealand. Ph.D. thesis, University of Auckland, Auckland, New Zealand.

Petersen, J.S., and Lofgren, G.E. (1986) Lamellar and patchy intergrowths in feldspar: Experimental crystallization of eutectic silicates. American Mineralogist, 71, 343–355.

Poldervaart, A., and Hess, H.H. (1951) Pyroxenes in the crystallization of basaltic magmas. Journal of Geology, 59, 472–489.

Smith, D. (1974) Pyroxene-olivine-quartz assemblages in rocks associated with the Nain anorthosite massif, Labrador. Journal of Petrology, 15, 58–78.

Statham, P.J. (1979) A ZAF procedure for microprobe analysis based on measurement of peak-to-background ratios. In D.E. Newbury, Ed., Microbeam analysis, p. 247–253. San Francisco Press, San Francisco.

Wager, L.R., and Brown, G.M. (1968) Layered igneous rocks. Oliver and Boyd, Edinburgh.

Walker, D., Kirkpatrick, R.J., Longhi, J., and Hays, J.F. (1976) Crystallization history of lunar picritic basalt sample 12002: Phase equilibria and cooling-rate studies. Geological Society of America Bulletin, 87, 646–656.

Manuscript received August 26, 1988
Manuscript accepted January 20, 1990